



3 1176 00165 9474

NASA CR-164,633

NASA-CR-164633  
19810019935

**COLLEGE  
OF  
ENGINEERING**

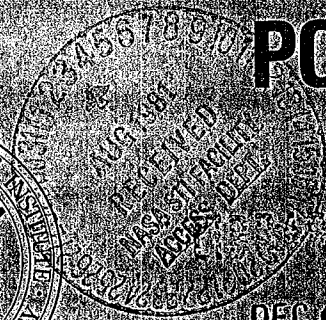
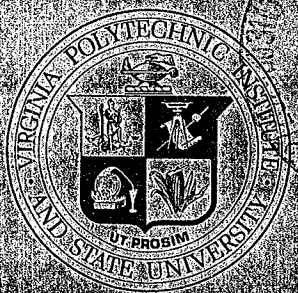
VPI-E-80-8

February, 1980

Convergence Rates for Finite Element Problems  
with Singularities

Part I - Antiplane Shear

Robert Plunkett<sup>1</sup>



**VIRGINIA  
POLYTECHNIC  
INSTITUTE  
AND  
STATE  
UNIVERSITY**

DEC 1980

**BLACKSBURG,  
VIRGINIA**



NF01144

College of Engineering  
Virginia Polytechnic Institute and State University  
Blacksburg, VA. 24061

VPI-E-80-8

February, 1980

Convergence Rates for Finite Element Problems  
with Singularities

Part I - Antiplane Shear

Robert Plunkett<sup>1</sup>

Department of Engineering Science and Mechanics

Interim Report 18 - NASA Grant CA #NCCI-15

Prepared for: Materials Application Branch  
National Aeronautics & Space Administration  
Langley Research Center  
Hampton, VA. 23665

<sup>1</sup>Visiting Professor  
Affiliation - Aerospace and Engineering Mechanics  
University of Minnesota

## ABSTRACT

The finite element method is widely used to find the stress fields caused by external loads and temperature changes in composite materials. This report presents the first of a set of systematic studies of the rate of convergence and effect of singularities on such solutions. The problem considered is that of a finite crack in an infinite medium under anti-plane shear load. For this problem, it is shown that the nodal force at the tip of the crack accurately gives the order of the singularity, that energy release methods can give the strength to better than 1% with element size 1/10 the crack length and that nodal forces give a much better estimate of the stress field than do the elements themselves.

This study is being extended to inplane shear, uniform tension and composite materials as well as finite bodies of rectangular form.

## TABLE OF CONTENTS

	<u>Page</u>
ACKNOWLEDGEMENTS . . . . .	iii
SECTION I. INTRODUCTION . . . . .	1
II. NUMERICAL SOLUTION . . . . .	2
III. RESULTS . . . . .	4
IV. CONCLUSIONS . . . . .	5
APPENDIX I. FINITE ELEMENT FORMULATION . . . . .	9
II. FACTORING TRIDIAGONAL MATRICES . . . . .	14
REFERENCES . . . . .	16
FIGURE 1a Stress fields . . . . .	18
1b Nodal force convergence . . . . .	18
2 Singularity-convergence vs. element size . . . . .	19
TABLE I . . . . .	20

## ACKNOWLEDGEMENTS

This work was accomplished during a sabbatical leave at VPI & SU with financial support from VPI & SU and the University of Minnesota. The author has benefitted greatly from conversations with Profs. C. T. Herakovich, J. L. Jenkins, M. P. Kamat and C. W. Smith.

## I. INTRODUCTION

The finite element method is widely used to find stress fields in non-homogeneous elastic materials, such as composites. For fracture analysis the most important information is usually the strength and nature of the singularity at the tip of a crack or at an interface between two laminae [e.g., 1,2]. Since the stress and strain fields are non-analytic at such singularities, it is difficult to improve the accuracy by the accepted procedure of averaging the stress or strain values in contiguous elements [3]. Pian and Tong [4] have shown that a minimum potential energy formulation gives nodal displacements which converge uniformly to the continuum solution for the displacement field. They and Perks [5,6] have discussed the convergence to the stress field in the vicinity of a singularity. The current method of choice is to fit the stress field near the tip by a region with a very fine mesh [7] or by using a special singular element [7,8]. The first method requires a large number of points and the second requires a prior knowledge of the nature of the singularity.

From Pian's work, it would appear that more information can be had from the nodal forces than has so far been exploited for static solutions; some work has already been done on finding energy release rates for both dynamic [9,10] and static problems [11,14].

A finite crack in an infinite elastic solid loaded at infinity in tension (Type I), plane shear (Type II) or antiplane shear (Type III) are useful subjects for investigation of convergence because they are conveniently modeled with rectangular elements, the resulting matrix equations may be solved with difference equation techniques, and the

solutions are well known for the homogeneous case. This report gives extensive results for antiplane shear; work continues on the other two loadings and on laminates.

## II. NUMERICAL SOLUTION

A finite element solution for strain field in an infinite solid with an infinite plane crack of width  $2c$  subjected to uniform antiplane shear at infinity is a set of nodal displacements  $w_{i,j}$  with the indices  $i,j$  going from  $-\infty$  to  $+\infty$ . If we put  $i = j = 0$  at the center of the crack, then  $w_{-i,j} = -w_{i,j}$  and  $w_{i,-j} = w_{i,j}$  so that we only need the solution for non-negative  $i$  and  $j$ . Solution details are given in Appendix I where it is shown that, for the residual problem, the nodal forces on the crack are  $f_{0j} = -1$ ,  $-N < j < +N$  and the displacements  $w_{0j} = 0$ ,  $|N| \leq |j|$ . We intend to investigate the effect of mesh size on the convergence of the solution; to do so, it is convenient to convert the above problem into the finite equivalent of a boundary integral problem by finding the finite equivalent of the Green's Function ( $N = 1$ ) and then using superposition.

Pian shows [4] that the displacement field defined by the nodal displacements and linear or bilinear element displacement fields (Appendix I) gives a total potential energy greater than that in the continuum if the boundary nodes are loaded by forces equal to

$$F_{0j} = \int_{j-1}^{j+1} w(\xi) \tau(\xi) d\xi \quad (1)$$

where  $w(\xi)$  is the (linearly varying) constrained displacement field.

For this to be valid, we must use the force boundary conditions of equation I-13b. In Appendix I, it is shown that the residual problem has a constant shear stress on the crack, so that the elements of  $f_0$  are all -1. We get the solution in two steps; the first step is to find the displacement field for  $w_{00} = 1$ ,  $w_{0j} = 0$ ,  $j \neq 0$ . From equations I-14 and I-17 in Appendix I:

$$w_{1j} = \frac{1}{N} \left( c_0/2 + \sum_{j=1}^{N-1} c_j \cos(jk\pi/N) + (-1)^j c_N/2 \right) \quad (2)$$

If we now let  $N \rightarrow \infty$

$$w_{1j} = \int_0^1 c(\xi) \cos \pi j \xi \, d\xi \quad (3)$$

where  $k\pi/N \rightarrow \pi\xi$  in equations I-16 and II-4. From equation II-2, it can be seen that

$$w_{ij} = \int_0^1 c^i(\xi) \cos \pi j \xi \, d\xi \quad (3)$$

so that the nodal displacement field can be found by numerical integration; we only need  $w_{1j}$  for our work.  $f_{00}$  is now found from equation I-6 or I-7; if we divide each element of  $\tilde{w}_1$  by  $f_{00}$  we have the first row of the displacement field for a unit force at  $i=0, j=0$  and  $f_0$  is found from equation I-13b. The linear (triangular element) and bilinear (rectangular) element values for  $f_{0 \cdot 200}$  agreed within  $4 \times 10^{-10}$  (0.01%) and agreed with the continuum value for  $\tau_{yz} = 1$  (Equation I-3) within  $5 \times 10^{-9}$ .

For crack length of 2N elements, we may write:

$$D_1 \tilde{w}_0^{(2N)} = f_0^{(2N)} \quad (4)$$

where  $f_0^{(2N)}$  is a column of 1's,  $2N-1$  long and  $D_1$  is a  $(2N-1) \times (2N-1)$  matrix each row of which is  $\tilde{f}_0^{(2)}$ , found from equation I-13b, with the  $f_{00}$  term on the main diagonal. Equation 4 can be reduced to  $N$  equations, since  $w_{0j} = w_{0,-j}$ , and solved for  $\tilde{w}_0$ . The nodal forces for  $N \leq j$  are now found by extending  $D_1$  into  $D_2$  and writing

$$D_2 \tilde{w}_0^{(2N)} = \hat{f}_0$$

where the elements of  $\hat{f}_0$  are  $f_{0,j}$ ,  $j \geq N$ .

### III. RESULTS

Using the bilinear rectangular elements, the nodal force at  $j = N+1$  is about 7.5% lower than  $\tau/\tau_0$  at  $x = N/N+1$ . For a constant  $x$ , this error decreases almost linearly with  $1/N$  so that linear extrapolation gives remarkably accurate results. For example, the finite element value for  $x = 1.25 c$  is 1.5962 for the 8 element solution and 1.6302 for 16. Linear extrapolation to  $1/M = 0$  gives 1.6643; the continuum value is 1.6667, an error of 0.14%. Figure 1A shows  $\tau_{yz}/\tau_0$  vs  $r/c$  as given by equations I-3 and I-4. It would be difficult to distinguish the finite element values from the exact curve for  $j > N+1$  but  $F_{N+1}$  is shown for  $N$  from 2 to 64. The trend for the constant strain (linear) elements is about the same but with about twice the error.

The above comparison shows, as is well known, that the nodal displacement values converge to the continuous displacement function at a rate appropriate to the order of the equivalent finite difference algorithm and that the stresses at any analytic point may be found by numerical differentiation of the displacement field to the same order

by using Hooke's law. Averaging the "stresses" in contiguous constant strain elements gives less accurate values unless the weighting points are carefully selected, e.g., the Gaussian integration points [3].

One would expect [4] the singular force at  $j = N$  to be given by the weighted integral of the stresses on the  $y = 0$  face from  $j = N-1$  to  $N+1$ . If we consider the original (not the residual) problem,  $\tau = 0$ ,  $j < N$ . Then using equation I-3 and a linear weighting function

$$\begin{aligned} F_N &= \frac{1}{h} \int_1^{1+h} \frac{x(1-x/h)}{\sqrt{x^2-1}} dx \\ &= \frac{\sqrt{8h}}{3} (1 + o(h)) \\ &= 0.9428 \sqrt{h} \end{aligned}$$

where  $h = 1/N$ . The continuum residual problem converted to finite element form differs from the residual finite element problem by adding  $0.5 h$  to  $F_N$ .

Since the displacement field solution is not analytic at the singularity, equations I-9 and I-11 don't apply. However, we are integrating only on a line where  $w = 0$  and  $\frac{\partial^2 w}{\partial x^2} = 0$  so that we may let  $w_{0j} = 0$  in these equations; if we use only  $w_{1,N-1}$ ,  $w_{1,N}$  and  $w_{1,N+1}$  we should get  $\frac{\partial w}{\partial y}$ ,  $o(h^4)$ . These and several other less accurate ( $o(h^2)$ ) approximations were used and they all converged very rapidly to  $c_1 \sqrt{h}$ . The points for the bilinear case are shown in Figure 1b. Rather than attempting to find the slope from the log-log plot, it is better to extrapolate  $F_N/\sqrt{h}$  vs  $h$  to  $h = 0$ . These curves are shown in figure 2 where we compare the nodal force at  $i = 0$ ,  $j = N$  using equation I-11 modified by letting  $w_{0,j} \equiv 0$ , the linear approximation for  $\frac{\partial w}{\partial y}$  and the second order approximation in which

we use  $\frac{\partial^2 w}{\partial x^2} + \frac{\partial^2 w}{\partial y^2} = 0$ . These algorithms are:

$$F_N = -\frac{1}{3} (w_{1,N-1} + w_{1,N} + w_{1,N+1}) \quad (\text{Eq I-11 mod}) \quad (5)$$

$$F_N = w_{1,N} = \frac{\partial w}{\partial y} + o(h^2) \quad (6)$$

$$F_N = -\frac{1}{6} (w_{1,N-1} + 4w_{1,N} + w_{1,N+1}) = \frac{\partial w}{\partial y} + o(h^4) \quad (7)$$

All of the curves converge to a square root singularity but the bilinear ones do so in a linear fashion which makes extrapolation accurate for crack lengths as coarse as 16 elements ( $N = 8$ ). Unfortunately, they don't extrapolate to the correct coefficient, which shows that higher order terms must be included even in the limit. Table I shows the rate of convergence for  $F_N$  to its value at  $h = 0$  using equation 7 for both the linear and bilinear case and to the square root singularity for equations 6 and 7.

The external work done is another measure of the strength of the singularity. The external work, equal to the strain energy, is

$$\begin{aligned} \pi/2 = U(c = 1) &= \int_{-1}^1 w(x) \tau_{yz}(x) dx \\ &\approx \frac{1}{N^2} \sum_{j=-N}^{N-1} w_{0j}(x) \text{ or Simpson's} \end{aligned} \quad (8)$$

because  $F_j = 1$ . As shown in Table 1, this converges as rapidly as  $F_N$ , and converges to the correct value. The columns headed  $\delta$  are the result of linear extrapolation using the entry and the previous entry; thus the extrapolation of  $U$  from the bilinear solution using 2 and 4 elements for the half crack length gives  $\pi/4$  with an error of 0.3%. One may also approximate the energy release rate from  $2 \cdot (w_{N-1} \cdot F_N/2)$ . This should

converge to

$$\frac{dU}{dc} = \pi c \quad (9)$$

The % error for the linear and bilinear case and for the extrapolated values are shown in the last four columns of Table I. These results are better than Rybicki [14] indicates.

Since the values for  $w_{0,50}^{(2)}$  agreed within  $5 \times 10^{-8}$  in the linear and bilinear cases and the small table top computer used in this work took about one minute per integration (equation 3), the values for  $j > 50$  from the linear case were used for the bilinear solutions. This small inconsistency accounts for the non-uniform convergence at levels of  $10^{-4}$  for  $N = 64$  in Table I.

#### IV. CONCLUSIONS

It has been shown that the singularity at a crack tip under antiplane shear (Type III) can be accurately modeled with a relatively coarse mesh near the tip if one uses the energy release from crack extension. The results are remarkably accurate if one gets solutions for two or three element sizes and extrapolates to zero size (Table I).

Curve fitting to the stress field requires a very fine mesh both because the slope of the continuum solution departs rapidly from that of the leading term and because the finite element solution is oscillating at the first two or three nodal points (see also Wilson [7]).

The nodal force at the crack tip as a function of mesh size is a very accurate measure of the order of the singularity but may converge to the wrong strength if higher order terms are not included. Even

where the displacement field is analytic, the nodal forces give a better approximation to the stress field than does element averaging.

The methods used in this report are being extended to Types I and II loading and laminated material and could be used for finite bodies of rectangular shape. They are economical with computer time since by using boundary element techniques, only small matrices need be inverted to get finite element solutions for large (or infinite) arrays. The results presented here were obtained on a small (64K bytes) table top computer.

## APPENDIX I - FINITE ELEMENT PROBLEM FORMULATION

Our problem is that of a crack of length  $-c \leq x \leq c$  in the  $y = 0$  plane, extending to  $\pm \infty$  in the  $z$  direction of the infinite solid with a uniform shear stress  $\tau_{yz} = \tau_0$  at  $x^2 + y^2 \rightarrow \infty$  (antiplane, Type III). This is the same problem as the edge crack of length  $c$  in the semi-infinite solid,  $x \geq 0$ . The continuum solution is given by Bentham and Koiter [12, Sect 3.3]. For antiplane shear:

$$\left. \begin{aligned} \tau_{xz} - \tilde{i} \tau_{yz} &= 2\phi'(\zeta) \\ \zeta &= x + \tilde{i}y \\ Gw &= \phi(\zeta) + \bar{\phi}(\zeta) \\ \tilde{i} &= \sqrt{-1} \end{aligned} \right\} \quad \text{I-1}$$

For our geometry:

$$\phi(\zeta) = -\frac{1}{2} \tilde{i} \tau_0 (\zeta^2 - c^2)^{1/2} \quad \text{I-2}$$

Along the  $x$  axis

$$\tau_{yz} = \tau_0 \left( \frac{x^2}{x^2 - c^2} \right)^{1/2} \quad x^2 > c^2 \quad \text{I-3}$$

There is a singularity of order  $1/2$  at  $x^2 = c^2$ . For  $r > 0$ , let

$$\left. \begin{aligned} x &= c + r, \quad \alpha = \frac{r}{c} \\ \text{Then } \tau_{yz} &= \tau_0 (2\alpha)^{-1/2} (1 + \frac{3}{4} \alpha + o(\alpha^2)) \\ \text{and } K_{III} &= \tau_0 c^{1/2} \end{aligned} \right\} \quad \text{I-4}$$

The finite element problem is more easily handled if we subtract a uniform stress field from the above, leaving a boundary condition of:

$$\left. \begin{array}{l} \tau_{yz} = -\tau_0 \quad y = 0 \quad , \quad x^2 < c^2 \\ \tau \rightarrow 0 \quad x^2 + y^2 \rightarrow \infty \end{array} \right\} \quad \text{I-5}$$

We use a square grid of nodal points at  $x = j$ ,  $y = i$  subjected to a shear stress  $\tau = 1$  on the negative face  $i = 0$ ,  $-c < j < c$  and let  $G = 1$ . By symmetry:

$$w_{-i,j} = -w_{i,j}$$

$$w_{i,-j} = w_{i,j}$$

The basic element is the square of side 1. By minimizing the strain energy [3] we can show that the nodal force at point  $i,j$  of the element(s) bounded by  $i$ ,  $i+1$ ,  $j$  and  $j+1$  is:

$$\tilde{F}_{ij} = w_{ij} - \frac{1}{2} w_{i+1,j} - \frac{1}{2} w_{i,j+1} \quad \text{I-6}$$

for a uniform strain field in the two triangular elements bounded either by the line  $(i,j)(i+1,j+1)$  or  $(i+1,j)(i,j+1)$ . It is interesting and useful that for antiplane shear the direction of the diagonal does not affect equation I-6. For the bilinear displacement field:

$$\begin{aligned} w = & w_{ij} (1-\zeta)(1-\eta) + w_{i+1,j} \zeta(1-\eta) \\ & + w_{i,j+1} (1-\zeta)\eta + w_{i+1,j+1} \zeta\eta \end{aligned}$$

the corresponding equation is:

$$\tilde{F}_{ij} = \frac{2}{3} w_{ij} - \frac{1}{6} w_{i+1,j} - \frac{1}{6} w_{i,j+1} - \frac{1}{3} w_{i+1,j+1} \quad \text{I-7}$$

These elements are now assembled to give a zero nodal force for  $i \neq 0$ .

Using equation I-6 the field equations are

$$F_{ij} = 0 = -w_{i-1,j} - w_{i,j-1} + 4w_{i,j} - w_{i,j+1} - w_{i+1,j} \quad \text{I-8}$$

and the nodal force on the negative y face is

$$F_{ij}^- = -\frac{1}{2} w_{i,j-1} + 2w_{i,j} - \frac{1}{2} w_{i,j+1} - w_{i+1,j} \quad \text{I-9}$$

Using equation I-7, they are

$$\begin{aligned} 0 = & -\frac{1}{3} (w_{i,j-1} + w_{i-1,j} + w_{i-1,j+1}) \\ & + (-\frac{1}{3} w_{i,j-1} + \frac{8}{3} w_{i,j} - \frac{1}{3} w_{i,j+1}) \\ & - \frac{1}{3} (w_{i+1,j-1} + w_{i+1,j} + w_{i+1,j+1}) \end{aligned} \quad \text{I-10}$$

and

$$\begin{aligned} F_{ij}^- = & -\frac{1}{3} (w_{i-1,j-1} + w_{i-1,j} + w_{i-1,j+1}) \\ & + \frac{1}{2} (-\frac{1}{3} w_{i,j-1} + \frac{8}{3} w_{i,j} - \frac{1}{3} w_{i,j+1}) \end{aligned} \quad \text{I-11}$$

Equation I-8 is the finite difference equation for the Laplacian good to  $o(h^2)$ ; using the governing partial differential equation

$$\frac{\partial^2 w}{\partial x^2} + \frac{\partial^2 w}{\partial y^2} = 0 \quad \text{I-12}$$

we find that equation I-9 gives the first derivative,  $w_y$ ,  $o(h^2)$ , while  $w_{i,j} - w_{i+1,j}$  is  $o(h)$ . Normally we can use  $\frac{1}{2} (w_{i-1,j} - w_{i+1,j})$  which is  $o(h^2)$  but not at a stressed surface. This same result does not hold for equations I-10 and 11 but we can show that the system converges  $o(h^4)$ .

The corresponding matrix equation is

$$-B\tilde{w}_{i-1} + A\tilde{w}_i - B\tilde{w}_{i+1} = 0 \quad \text{I-13a}$$

$$E\tilde{w}_0 - F\tilde{w}_1 = \frac{1}{2} A\tilde{w}_0 - B\tilde{w}_1 = \tilde{f}_0 \quad \text{I-13b}$$

where  $\tilde{w}_i$  is the column vector of the displacements of the nodes in  $i^{\text{th}}$  row. Using the notation of Appendix II, the values of a and b in equation II-1 are those in Table I.

Equation Matrix	I-8		I-9		I-10		I-11	
	A	B	E	F	A	B	E	F
a	4	-1	2	-1	8/3	-1/3	4/3	-1/3
b	-1	0	-1/2	0	-1/3	-1/3	-1/6	-1/3

Table I-1

We may solve the matrix difference equation I-13a, by expanding  $\tilde{w}_i$  in the eigenvectors of Appendix II. Using equation II-7, if we substitute:

$$\left. \begin{aligned} \tilde{w}_i &= \underline{X} \tilde{q}_i \\ A &= \underline{X} \Lambda_A \underline{Y} \\ B &= \underline{X} \Lambda_B \underline{Y} \end{aligned} \right\} \quad \text{I-14}$$

into equation I-13a and use the last of equations II-2, the equations for  $\tilde{q}_i$  are decoupled:

$$-\Lambda_B \tilde{q}_{i-1} + \Lambda_A \tilde{q}_i - \Lambda_B \tilde{q}_{i+1} = 0 \quad \text{I-15}$$

If we now let:

$$\left. \begin{aligned} q_{ik} &= c_k q_{i-1,k} \\ \text{then} \quad -\lambda_{Bk} c_k^{-1} + \lambda_{Ak} - \lambda_{Bk} c_k &= 0 \\ \text{and} \quad c_k &= \beta_k \pm \sqrt{\beta_k^2 - 1} \\ \text{where} \quad \beta_k &= \lambda_{Ak} / 2\lambda_{Bk} \end{aligned} \right\} \quad \text{I-16}$$

$\lambda_{Ak}$  and  $\lambda_{Bk}$  are given by equation II-4 and a and b are shown in table I-1. In order to satisfy the condition at infinity, we take the + or - sign to make  $c^2 < 1$ .  $c_k \rightarrow 1/2 \beta$  as  $\beta^{-1} \rightarrow 0$ .

If  $w_{00} = 1$ ,  $w_{0j} = 0$ ,  $j \neq 0$ , from equations I-13a and I-16

$$\lambda_{Ak} q_{ik} - \lambda_{Bk} q_{2k} = \lambda_{Bk} x_{ok} w_{00} = \lambda_{Bk} w_{00}$$

$$(\lambda_{Ak} - c \lambda_{Bk}) q_{ik} = \lambda_{Bk} w_{00}$$

or

$$q_{ik} = c_k w_{00}$$

I-17

## APPENDIX II - FACTORING TRIDIAGONAL MATRICES

The matrices we are concerned with all have one constant,  $a$ , on the main diagonal and another,  $b$ , on the first sub and superdiagonal with all other elements zero. By symmetry, they extend from  $-N$  to  $+N$  and are  $(2N+1) \times (2N+1)$  square. In order to get symmetrical reflection at  $\pm N$ , we make the second element of the first row and the next to the last element of the last row equal to  $2b$  which gives the following form.

$$R = \begin{bmatrix} a & 2b & 0 & 0 & \cdot & \cdot & \cdot \\ b & a & b & 0 & \cdot & \cdot & \cdot \\ 0 & b & a & b & \cdot & \cdot & \cdot \\ \cdot & \cdot & \cdot & \cdot & \cdot & \cdot & \cdot \\ \cdot & \cdot & \cdot & \cdot & \cdot & \cdot & \cdot \\ \cdot & \cdot & \cdot & \cdot & \cdot & \cdot & \cdot \\ \cdot & \cdot & \cdot & \cdot & 0 & 2b & a \end{bmatrix} \quad \text{II-1}$$

The associated eigenvalue problem is:

$$\left. \begin{aligned} R\bar{X} &= \bar{X}\Lambda \\ \bar{Y}R &= \Lambda\bar{Y} \\ \bar{Y}\bar{X} &= I \end{aligned} \right\} \quad \text{II-2}$$

normalized to

$$R = \bar{X}\Lambda\bar{Y} \quad \text{and} \quad \bar{Y}R\bar{X} = \Lambda$$

so that

where  $\Lambda$  is the diagonal matrix of the eigenvalues,  $\bar{X}$  is the square matrix of the eigenvector columns and  $\bar{Y}$  is the adjoint square matrix of the eigenvector rows. The difference equations are:

$$\left. \begin{aligned} b x_{i-1,k} + a x_{i,k} + b x_{i+1,k} &= \lambda_k x_{i,k} \\ a x_{-N,k} + 2b x_{-N+1,k} &= \lambda_k x_{-N,k} \\ 2b x_{N-1,k} + a x_{N,k} &= \lambda_k x_{N,k} \end{aligned} \right\} \quad \text{II-3}$$

The matrix has  $2N+1$  roots:

$$\lambda_k = a + 2b \cos (k\pi/2N) \quad k = 0,1,\dots,2N+1 \quad \text{II-4}$$

The corresponding column eigenvectors are:

$$x_{ik} = \cos (ik /2N) \quad i = -N,\dots,0,\dots,N \quad \text{II-5}$$

The adjoint row eigenvectors are:

$$Y_{ki} = (1 - \frac{1}{2} \delta_{i,\pm N})(1 - \frac{1}{2} \delta_{\pm N,k})x_{ik}/N \quad \text{II-6}$$

where  $\delta_{ij}$  is the Kronecker  $\delta$ .

The antisymmetric tridiagonal matrix found by replacing the  $2b$  terms in equation II-1 with 0, has the same eigenvalues, but sines for the eigenvectors (equation II-5) instead of cosines.

## REFERENCES

1. Herakovich, C. T., A. Nagarkar and D. A. O'Brien, "Failure Analysis of Composite Laminates with Free Edges," in Modern Development in Composite Materials and Structures, J. S. Vinson, ed. ASME, 53-66, 1979.
2. Reifsnider, K. L., "Mechanics of Failure of Composite Materials," Proc. Int'l. Symp. on Fracture Mech., ONR/GWU, Wash., D.C., 1978.
3. Zienkiewicz, O. C., "The Finite Element Method," McGraw-Hill (U.K.) 3rd ed., 1977.
4. Pian, T. H. H. and P. Tong, "Basis of Finite Element Methods for Solid Continua," Int. J. Num. Methods in Engineering, 1, 1, 3-28 (1969).
5. Tong, P. and T. H. H. Pian, "On the Convergence of the Finite Element Method for Problems with Singularity," Int. J. Solids and Structures, 9, 313-321 (1973).
6. Perkes, D. M., "On the Convergence of Finite Elements in the Presence of Singularities," Int. J. Num. Methods in Engineering, 14, 5, 780-784 (1979).
7. Wilson, W. K., "Finite Element Methods for Elastic Bodies Containing Cracks," in Methods of Analysis and Solutions of Crack Problems, G. L. Sih, ed., Noordhoff, 484-515, 1973.
8. Atluri, S. N., T. Nishioka and M. Nakagaki, "Numerical Modeling of Dynamic Crack Propagation by Moving Singular Elements," in Nonlinear and Dynamic Fracture Mechanics, N. Perrone and S. Atluri, eds., AMD-31, ASME, 37-66, 1979.
9. Caldis, E. S., D. R. J. Owen and O. C. Zienkiewicz, "Nonlinear Dynamic Transient Methods in Crack Propagation Studies," in AMD-31, ASME, 1-18 [see 8].
10. Kobayashi, A. S., "Dynamic Fracture Analysis by Dynamic Finite Method," in AMD-31, ASME, 19-36 [see 8].
11. Wang, A. S., F. W. Crossman and G. E. Law, "Interlaminar Failure in Epoxy Based Composite Laminates," in Advanced Composites: Design and Applications, T.R. Shives and W. A. Willord eds, NBS Spec. Pub. 563, Washington, D.C., 1979.
12. Bentham, J. P. and W. T. Koiter, "Asymptotic Approximations to Crack Problems," in Methods of Analysis and Solutions of Crack Problems, G. C. Sih, ed., Noordhoff, 131-178, 1973.

13. Abramovitz, M., and I. A. Stegun, "Handbook of Mathematical Functions," N.B.S. 1962 or Dover 1976.
14. Rybicki, E. F., and M. F. Kanninen, "Finite Element Calculation of Stress Intensity Factors by a Modified Crack Closure Integral," Eng. Fract. Mech., 9, 1977, pp. 931-38.

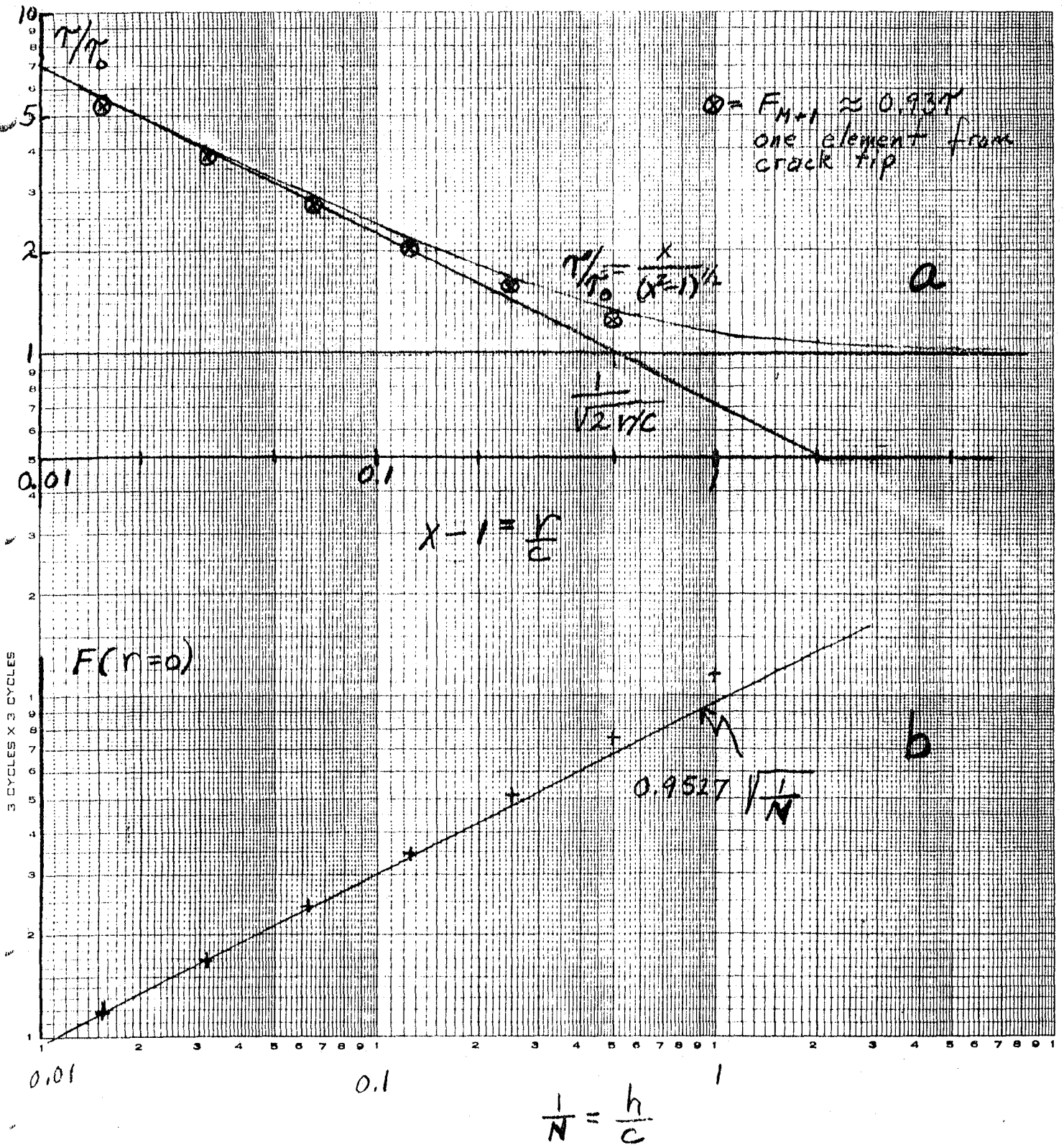


Figure 1a. Stress fields.

Figure 1b. Nodal force convergence.

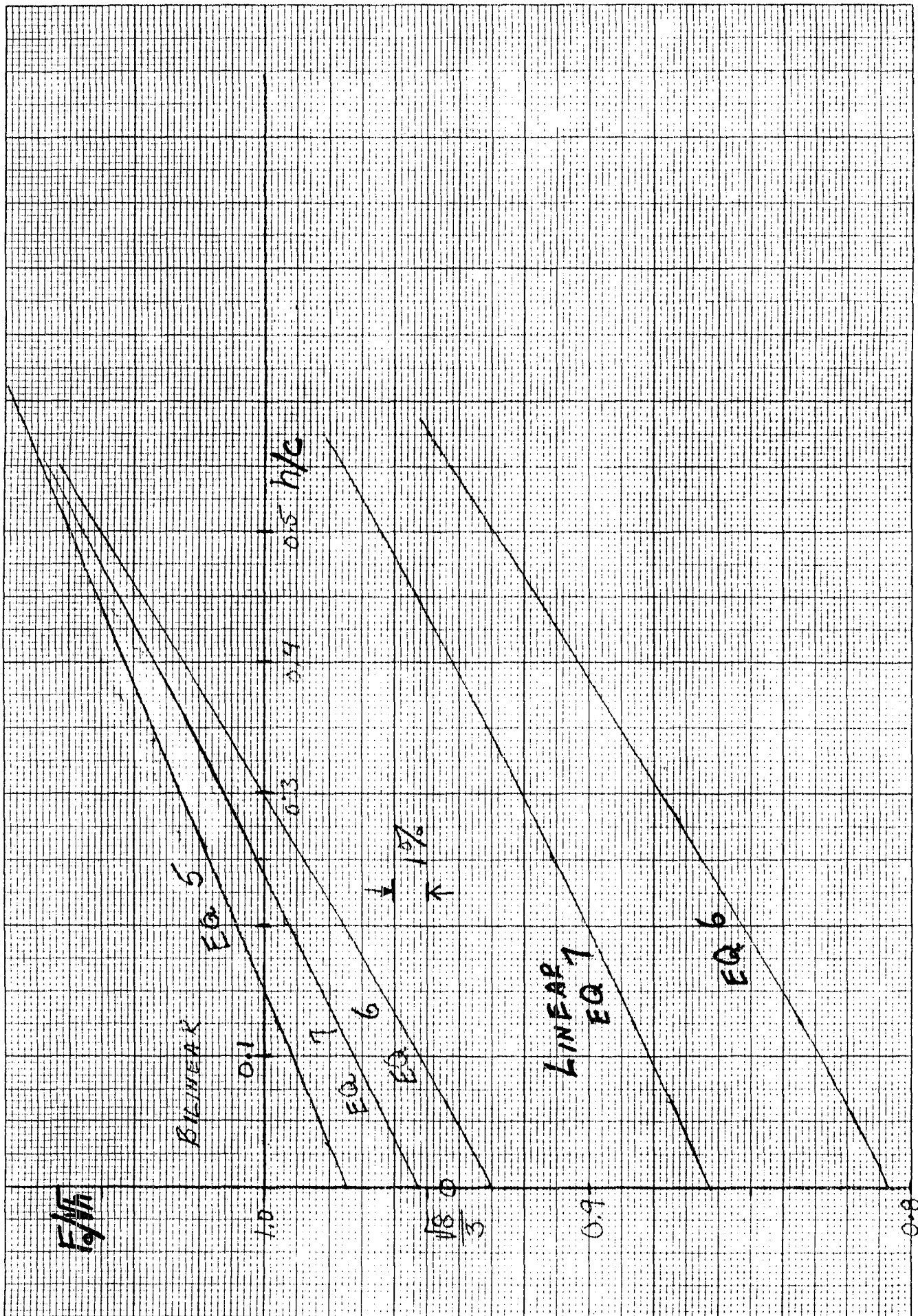


Figure 2. Singularity-convergence vs. element size.

$$\% \text{ CONVERGENCE} = 100 \frac{|X_{00} - X_M|}{X_{00}}$$

c/h M	F <sub>N</sub> (r = 0)		τ = r <sup>-α</sup> α		Bilinear		Bilinear		Linear		Bilinear		Linear	
	Bi o(h) <sup>4</sup>	Linear o(h) <sup>4</sup>	o(h <sup>4</sup> )	δ	o(h <sup>2</sup> )	δ	U	δ	U	δ	F <sub>N</sub> <sup>w<sub>N-1</sub></sup>	δ	F <sub>N</sub> <sup>w<sub>N-1</sub></sup>	δ
1	22.4	27.4	---	---	---	---	32	---	61	---				
2	10.8	11.8	28.5	---	34.3	---	21	10.2	33.4	6.0	11.9		19.9	
4	5.2	5.9	14.8	1.2	17.8	1.2	10.3	0.30	17.2	1.1	5.5	0.9	9.3	1.28
8	2.6	2.8	7.4	0.02	8.8	0.06	5.1	0.07	8.7	0.22	2.7	0.21	4.5	0.24
16	1.3	1.4	3.7	0.06	4.4	0.10	2.6	0.03	4.4	0.05	1.3	0.05	2.24	0.05
32	0.6	0.7	1.8	0.01	2.2	0.04	1.3	0.004	2.2	0.013	0.6	0.012	1.11	0.013
64	0.3	0.3	0.9	0.04*	1.1	0.03*	0.6	0.007*	1.1	0.004	0.3	0.018*	0.55	0.004
	(a)		(b)				(c)				(d)			

(a) linear  $h \rightarrow 0$  ,  $F_{\infty} = 0.953$

$$\sqrt{8}/3 = 0.943$$

(b) linear  $h \rightarrow 0$  ,  $F_{\infty} = 0.862$

(c)  $U_{\infty} = \pi/2$  ,  $\alpha_{\infty} = 1/2$

(d)  $F_{N}^{w_{N-1}} \rightarrow \pi/2N$

\* Inaccurate to  $10^{-4}$

TABLE I

Prof. Donald F. Adams  
Dept. Of Mechanical Engineering  
University Of Wyoming  
Laramie, WY 82070

Dr. N. R. Adsit  
General Dynamics Convair  
P.O. Box 80837  
San Diego, CA. 92138

Dr. J. A. Bailie  
D81-12 Bldg. 154  
Lockheed Missiles & Space Co, Inc  
1111 Lockheed Way  
Sunnyvale, CA. 94088

Mr. Henry W. Bergner, Jr.  
The Boeing Company  
Mail Stop 3707  
Seattle, WA. 98124

Dr. Charles W. Bert, Director  
School Of Aerospace, Mechanical  
& Nuclear Engineering  
The University Of Oklahoma  
Norman, Oklahoma 73069

Mr. Richard Boitnott  
Mail Stop 188a  
Nasa-Langley Research Center  
Blacksburg, Va. 24061

Mr. David Bowles  
Mail Stop 188B  
NASA-Langley Research Center  
Hampton, Va. 23665

Dr. H. F. Brinson  
ESM Dept.  
VPI&SU  
Blacksburg, VA. 24061

Dr. Michael F. Card  
Mail Stop 190  
NASA-Langley Research Center  
Hampton, VA 23665

Dr. C. Chamis  
NASA-Lewis Research Center  
2100 Brook Park Rd.  
Cleveland, Ohio 44135

Dr. Paul A. Cooper  
Mail Stop 190  
NASA-Langley Research Center  
Hampton, Va. 23665

Dr. Frank Crossman  
Lockheed Research Lab  
Org. 52-41, Bldg. 204  
3251 Hanover Street  
Palo Alto, CA. 94304

Dr. I. M. Daniel, Manager  
IIT Research Institute  
10 West 35 Street  
Chicago, IL. 60616

Dr. John R. Davidson  
Mail Code 188E  
MD-Structural Integrity Branch  
Langley Research Center  
Hampton, VA. 23665

Dr. John G. Davis, Jr.  
Mail Stop 188A  
Langley Research Center  
Hampton, VA. 23665

Mr. Jerry W. Deaton  
Mail Stop 188A  
NASA-Langley Research Center  
Hampton, VA. 23665

Mr. H. Benson Dexter  
Mail Stop 188A  
NASA-Langley Research Center  
Hampton, VA. 23665

Mr. O. Earl Dhonau  
Section 2-53400  
Vought Corp.  
P.O. Box 5907  
Dallas, TX. 75222

Dr. S. C. Dixon  
Mail Stop 395  
NASA-Langley Research Center  
Hampton, VA. 23665

Dr. J. E. Duberg  
Mail Stop 103  
NASA-Langley Research Center  
Hampton, Va. 23665

Dr. M. F. Duggan  
52-33/205/2  
Lockheed Palo Alto Lab.  
3251 Hanover St.  
Palo Alto, Ca. 94304

Dr. Wolf Elber  
Mail Stop 188E  
NASA-Langley Research Center  
Hampton, VA. 23665

Mr. Gary L. Farley  
Mail Stop 188A  
NASA-Langley Research Center  
Hampton, VA. 23665

Mr. Larry Fogg  
Lockheed-California  
Dept. 7572, Bldg. 63, Plant A1  
P.O. Box 551  
Burbank, CA. 91520

Dr. R. L. Foye  
USAMRDL  
SAUDLAS (207-5)  
Moffet Field, CA. 94035

Dr. D. Frederick  
ESM Dept.  
VPI&SU  
Blacksburg, VA. 24061

Mr. Samuel P. Garbo  
McDonnell Aircraft Co.  
Bldg. 34, Post 350  
St. Louis, MO. 63166

Mr. Ramon Garica  
Mail Stop 190  
NASA-Langley Research Center  
Hampton, VA. 23665

Dr. Login B. Greszczuk  
McDonnell Douglas Astr. Co.  
5301 Bolas Avenue  
Huntington Beach, CA. 92647

Mr. Glen C. Grimes, Engr. Spec.  
Structures R & T, Dept 3780/62  
Northrop Corp., Aircraft Div.  
3901 W. Broadway  
Hawthorne, CA. 90250

Dr. H. T. Hahn  
Washington University  
St. Louis, MO. 63130

Dr. J. C. Halpin  
Flight Dynamics Lab  
Wright-Patterson AFB  
Ohio 45433

Professor Z. Hashin  
School of Engineering  
Dept. of Solid Mech. Materials  
and Structures  
Tel Aviv University  
Tel Aviv, Israel

Dr. R. A. Heller  
ESM Dept.  
VPI&SU  
Blacksburg, VA. 24061

Dr. E. G. Henneke  
ESM Dept.  
VPI&SU  
Blacksburg, VA. 24061

Professor Phil Hodge  
107 Aeronautical Engr. Bldg.  
University of Minnesota  
Minneapolis, MN 55455

Dr. K. E. Hofer  
IIT Research Institute  
10 West 35 Street  
Chicago, Illinois 60616

Mr. Edward L. Hoffman  
Mail Stop 188A  
NASA-Langley Research Center  
Hampton, VA. 23665

Dr. Peter W. Hsu  
Mail Stop 1-1-12  
Hamilton Standard Division  
Windsor Locks, CT. 06096

Mr. Edward A. Humphreys  
Materials Science Corporation  
Blue Bell Office Campus  
Blue Bell, PA. 19422

Dr. Michael W. Hyer  
ESM Dept.  
VPI&SU  
Blacksburg, VA. 24061

AVCO, Systems Division  
Subsystems & Meth. Structures  
201 Lowell Street  
Wilmington, MA. 01887

Dr. Eric R. Johnson  
ESM Dept.  
VPI&SU  
Blacksburg, VA. 24061

Dr. N. J. Johnson  
Mail Stop 226  
NASA-Langley Research Center  
Hampton, VA. 23665

Dr. M. P. Kamat  
ESM Dept.  
VPI&SU  
Blacksburg, VA. 24061

Dr. Keith T. Kedward  
1768 Granite Hills Dr.  
El Cajon, CA. 92021

Mr. John M. Kennedy  
Mail Stop 188E  
NASA-Langley Research Center  
Hampton, VA. 23665

Mr. James F. Knauss  
Section 2-30400  
Vought Corp.  
P.O. Box 225907  
Dallas, TX. 75265

Dr. Ronald D. Kriz  
Dept. Com. NBS Bldg. 2  
Boulder, CO. 80302

Dr. S. V. Kulkarni  
L342 Lawrence Livermore Lab  
P. O. Box 808  
Livermore, Ca. 94550

Dr. M. R. Louthan  
Materials Engineering  
VPI&SU  
Blacksburg, VA. 24061

Mr. Vic Mazzio  
General Electric Co.  
P.O. Box 8555  
Bldg. 100, Rm. M4018  
Philadelphia, PA. 19101

Mr. Robert R. McWithey  
Mail Stop 190  
NASA-Langley Research Center  
Hampton, VA. 23665

Dr. Martin M. Mikulas  
Mail Stop 190  
NASA-Langley Research Center  
Hampton, VA. 23665

Mr. J. Steve Mills  
6100 Edinger Ave., Apt. 525  
Huntington Beach  
CA 92647

Dr. D. H. Morris  
ESM Dept.  
VPI&SU  
BLACKSBURG, VA. 24061

Mr. Anya Nagarkar  
Material Sciences Corp.  
Blue Bell Office Campus  
Blue Bell, PA. 19422

NASA Scientific & Technical  
Information Facility  
P.O. Box 8757  
Baltimore/Washington Inter. Air.  
Baltimore, MD. 21240

Newman Library - VPI&SU

Mr. David A. O'Brien  
5902 Kingsford Pl.  
Bethesda, MD 20034

Dr. Donald W. Oplinger  
Army Materials & Mechanics  
Research Center  
Department of the Army  
Watertown, MA. 02171

Dr. Nicholas J. Pagano  
WPAFB/MBM  
Wright Patterson AFB  
Ohio 45433

Dr. Nicholas Perrone, Director  
Structural Mechanics Program  
Department of the Navy  
Office of Naval Research  
Arlington, VA. 22217

Prof. T. H. H. Pian  
Mass. Inst. of Tech.  
Dept. of Aero. & Astr.  
Cambridge, MA. 02139

Mr. Marek-Jerzy Pindera  
Mail Stop 188A  
NASA-Langley Research Center  
Hampton, VA. 23665

Dr. R. Byron Pipes  
Dept. of Mech. & Aero. Engr.  
107 Evans Hall  
University of Delaware  
Newark, DE. 19711

Dr. K. L. Reifsnider  
ESM Dept.  
VPI&SU  
Blacksburg, VA. 24061

Dr. Gary D. Renieri  
McDonnell Douglas Astro. Co-East  
P.O. Box 516  
Bldg. 106, Level 4, Post C-5  
St. Louis, MO. 63166

Dr. Michael W. Renieri  
McDonnell Aircraft Co.  
Bldg. 34, Post 350  
St. Louis, MO. 63166

Dr. Larry Roderick  
Mail Stop 188E  
NASA-Langley Research Center  
Hampton, VA. 23665

Dr. B. W. Rosen  
Materials Science Corporation  
Blue Bell Office Campus  
Blue Bell, PA. 19422

Dr. R. E. Rowlands  
Dept. of Engineering Mechanics  
University of Wisconsin  
Madison, WI. 53706

Dr. Edmund F. Rybicki  
Battelle  
Columbus Laboratories  
505 King Avenue  
Columbus, OH. 43201

Mr. Harminder Saluja  
Boeing Vertol Company  
Structural Technology  
P.O. Box 16858  
Philadelphia, PA. 19142

Dr. J. Wayne Sawyer  
Mail Stop 190  
NASA-Langley Research Center  
Hampton, VA. 23665

Dr. George P. Sendekyj  
Structures Division  
Air Force Flight Dynamics Lab.  
Wright-Patterson AFB  
Ohio 45433

Mr. Mark J. Shuart  
Mail Stop 188  
NASA-Langley Research Center  
Hampton, VA. 23665

Dr. James H. Starnes, Jr.  
Mail Stop 190  
NASA-Langley Research Center  
Hampton, VA. 23665

Prof. Yehuda Stavsky  
Gerard Swope Prof. of Mech.  
Technion-Israel Inst. of Tech.  
Technion City, Haifa, Israel

Dr. W. W. Stinchcomb  
ESM Dept.  
VPI&SU  
Blacksburg, VA. 24061

Dr. Darrel R. Tenney  
Mail Code 188B  
MD-Materials Research Branch  
Langley Research Center  
Hampton, VA. 23665

Dr. S. W. Tsai  
Nonmetallic Materials Division  
Air Force Materials Laboratory  
Wright-Patterson AFB  
Ohio 45433

Dr. J. R. Vinson  
6242 Urey Hall  
Applied Mechanics & Science Dept  
Univ. of California-San Diego  
La Jolla, CA. 92037

Mr. M. E. Waddoups  
General Dynamic Corp.  
Fort Worth, TX 76101

Dr. T. A. Weisshaar  
Aero & Ocean Engr. Dept.  
VPI&SU  
Blacksburg, VA. 24061

Dr. J. M. Whitney  
Nonmetallic Materials Division  
Air Force Materials Laboratory  
Wright-Patterson AFB  
Ohio 45433

Mr. Thomas A. Zeiler  
Mail Stop 395  
NASA-Langley Research Center  
Hampton, VA. 23665

Dr. Carl H. Zweben  
General Electric Co.  
Space Division  
P.O. Box 8555  
Philadelphia, PA. 19101

**End of Document**